Hindawi
Mathematical Problems in Engineering
Volume 2020, Article ID 2534038, 13 pages
https://doi.org/10.1155/2020/2534038

Research Article

Echo State Network for Extended State Observer and Sliding Mode Control of Vehicle Drive Motor with Unknown Hysteresis Nonlinearity

Xuehui Gao,[1] **Bo Sun**,[1] **Xinyan Hu**,[1] **and Kun Zhu**[2]

[1]*The Department of Mechanical and Electrical Engineering, Shandong University of Science and Technology, Tai'an 271019, China*
[2]*Traffic Control Technology Co. Ltd., Beijing 100071, China*

Correspondence should be addressed to Bo Sun; bo_sun@sdust.edu.cn

Received 27 November 2019; Accepted 12 December 2019; Published 4 January 2020

Guest Editor: Weicun Zhang

An echo state network (ESN) for extended state observer (ESO) and sliding mode control (SMC) of permanent magnet synchronous motor (PMSM) in an electric vehicle system is investigated in this paper. For the PMSM model, most researches neglect the hysteresis loss and other nonlinear factors, which reduces the accuracy of the PMSM model. We present a modified PMSM model considering the hysteresis loss and then transform the new PMSM model to a canonical form to simplify the controller design. In order to deal with the hysteresis loss, an ESN is utilized to estimate the nonlinearity. Considering that some states cannot be directly obtained, an ESO with ESN is proposed to estimate unknown system states of the electric vehicle PMSM system. Afterwards, an SMC is adopted to control the closed-loop system based on the ESO with ESN, and a double hyperbolic function instead of the sign function is used to suppress the chattering of the SMC. The stabilities of the observer and the controller are all guaranteed by Lyapunov functions. Finally, simulations are presented to verify the validity of the echo state network for extended state observer and the neural network sliding mode control.

1. Introduction

Electric vehicles are the most important new energy resource vehicles that attract much attention in these years. Many researchers and factories have investigated the electric vehicles and got some well results. Different electric vehicles have been produced, and some have been accepted in the market. Even though the electric vehicles already appeared in the market, they also have a lot of problems that need to be investigated. For example, an accurate electric vehicle motor model is one of the important issues that needs to be investigated more such that it can improve the precision of the control system and the automation for electric vehicles.

Most of the electric vehicles adopt permanent magnet synchronous motor (PMSM), and their models have been investigated for many years. But the electric vehicles not only include the PMSM but also have many other subsystems such as torque production dynamics and crankshaft dynamics. Na et al. [1] discussed the different models of vehicle and designed an input observer and adaptive estimations to approximate the unknown parameters. In order to precisely control the tracking errors, Na et al. [2] utilized the prescribed performance function to control the vehicles suspensions. Wang et al. [3, 4] designed an adaptive controller to precisely control the model of PMSM with funnel motion control that is similar to that in literature [2]. Huang et al. [5] proposed an approximation-free control strategy which does not need function approximators (e.g., neural networks and fuzzy logic systems) for the vehicles suspension [2]. Furthermore, Na et al. [6] investigated the nonlinear active suspension systems of vehicles with adaptive finite time

fuzzy control strategy considering the input delay since the input delay commonly appears in the suspension systems of vehicle. And in literature [7], the autonomous vehicles were researched with extended Kalman filter designing minimum model error tracking control that considers the input saturation in real vehicle systems that always contains the issue of the input saturation. Compared with many other literatures that utilized linear tyre model, Li et al. [8] had investigated the nonlinear tyre model with vehicle MP algorithm. Sun et al. [9, 10] investigated the variable stiffness and damping model of magneto-rheological (MR) vehicle suspension system. The MR damper is described by two Bouc–Wen hysteretic models, and TS fuzzy approach was used to model the quarter car system.

All the above studies investigated the vehicles' model or part of vehicles' model (submodel), but these vehicle systems are not just pure electric vehicle systems, which also include hybrid electric vehicle systems. In pure electric vehicle systems, the motor model is the most important model such that it draws much attention. Many kinds of motor can be utilized for electric vehicles, and the permanent magnet synchronous motors (PMSMs) are the common motors in the vehicle systems. The PMSM model has been investigated for many years, and different approaches were applied for different conditions. Luo et al. [11] proposed a field-circuit-coupled parameter adaptive modeling method for PMSM which combined the merits of a mathematical model and a magnetic field model. Since the permanent magnet materials in the electric vehicles have hysteresis losses in practice, it has been investigated in different applications and many results were acquired. Egorov et al. [12] investigated the hysteresis loss of the permanent magnet using static history-dependent hysteresis model (HDHM) for PMSM with ferrite magnets of a rotor surface magnet. But in literature [13], a zero-sequence current hysteresis controller with space vector pulse-width modulation was presented to solve the system loss of the open-end winding permanent magnet synchronous motor, where the loss was caused by the limited maximum output power. Notwithstanding the hysteresis of the PMSM is widely researched [14, 15], and it also has much issues to be further researched such as using mathematical hysteresis models or intelligent models to describe the hysteresis or using an observer to estimate the unable direct measurement hysteresis parameters. Considering the U model theory [16–19], the structure of the model and the observer is presented under the inspiration of the model-independent framework for the U model. Therefore, the observer and the controller will be investigated based on the U model model-independent framework.

Many real electric vehicle systems cannot obtain all the model states directly, and then the observer will be utilized to estimate the unknown states or parameters. In general, the observer is utilized to estimate two categories of unknowns in controlled systems: disturbances and states [4, 20–24]. Many different observers have been applied to approximate the states or disturbances for many years. In these observers, the extended state observer (ESO) is one of the excellent observers and has achieved well results. ESO is firstly proposed by Han [25], and it has been further researched by many excellent scholars. Xue et al. [26] proposed an ESO-based active disturbance rejection control (ADRC) to deal with the uncertainties of the system, where the ESO gain could automatically timely be adjusted for reducing the estimation errors. Xue et al. [27] proved that a certain ESO could serve as estimation through the augmented gain. Chen et al. [28] proposed an ESO to estimate both the high-order nonlinear system unknown states and uncertainties in order to facilitate the controller design. Sun et al. [29] focused on the multimotor servomechanism systems, using the ESO to approximate the unmeasured velocity of servo motors, and Wang et al. [30] also investigated the motor servomechanism systems, but it is different to [29]. The ESO was utilized to estimate the unknown dynamics in the control system (e.g., friction and disturbances) for its easy design on account of the system bandwidth. On the whole, most ESOs are utilized to estimate the "total disturbance," which is regarded as the disturbance observer for the control systems. But in this paper, we will adjust the structure of the ESO to approximate the system states. The adjusted structure of ESO has designed high gain parameters that can fastly estimate the unknown system states and higher accuracy. In order to simplify the ESO design and guarantee the ESO convergence, the hysteresis nonlinearity of the PMSM model and other unknown sections as "general disturbance" will be handled by a proposed echo state network (ESN).

ESN has been utilized for many nonlinear systems for its fewer nodes and computational requirements. Chen et al. [31] designed an adaptive ESN control for a class of constrained pure-feedback nonlinear systems, but Sun et al. [32] investigated a modified ESN dynamic surface controller for multi-input and multioutput nonlinear systems. These ESNs all have acquired well results. In additions, Wang et al. [33, 34] investigated the prescribed performance tracking control of nonlinear servo mechanisms with ESN, one chose robust adaptive control and the other selected dynamic surface control and verified by experiments. Different from the above literatures, Wang et al. [35] researched the two-inertia servo mechanisms using ESN and designed a prescribed performance function dynamic surface control. Wang et al. [34] considered the influence of the backlash for the servo mechanisms. Different from [34] that utilized ESN to dispose the backlash nonlinearities, we will adopt ESN to deal with the unknown hysteresis nonlinear sections using the ESO simplifying the ESO design in this paper.

Sliding mode control (SMC) is one of the excellent control strategies which can be frequently used in practice. We have utilized a composite control which consists of a discrete inverse model-based control and a discrete adaptive sliding mode control to deal with a Hammerstein system in literature [36]. The Hammerstein system was composed of a linear dynamics connecting a hysteresis nonlinearity, where the order of linear dynamics was unknown and the hysteresis modeled by Preisach operator. Then, the effectiveness of the sliding mode control was verified by servo motor system experiments. In order to restrain the chattering of the sliding

mode control, Gao et al. and Tao et al. [36, 37] adopted double hyperbolic function $\tanh(\cdot)$ instead of the $\text{sign}(\cdot)$, which can obtain favourable reduced chattering. The sliding mode control is applied for many real systems. Zhao et al. [38] applied the SMC to the multimotor driving servo systems, and Chen et al. [39] utilized the SMC for an uncertain spacecraft system. In the literature [7], the sliding mode control was used for the autonomous vehicles. In this paper, the SMC will be designed to precisely control the proposed PMSM model system where the unknown states are estimated by the adjusted ESO with ESN.

In this paper, we firstly consider the influence of the hysteresis nonlinearity for the PMSM model that mostly is neglected in the former models. Therefore, a new modified PMSM model including the hysteresis nonlinearities is established. Secondly, the modified PMSM model will be transformed to a canonical form to simplify the controller design. Then, the ESN is applied, and a new ESO will be proposed to estimate all the states whether that can be directly measured or not. A Lyapunov function guarantees the effectiveness of the observer results. Finally, an SMC with the ESN and the ESO is designed for this new modified PMSM model, and another Lyapunov function guarantees all the closed-loop signals bounded. In order to restrain the chattering of the SMC, we chose the continuous function $\tanh(\cdot)$ replacing the discontinuous function $\text{sign}(\cdot)$ and the simulations will verify the effectiveness of the proposed approaches. The contributions are listed as follows:

(i) The PMSM model is improved for suiting the electric vehicle system which considers the hysteretic losses. Besides, the modified PMSM model is transformed to a canonical form that can simplify the ESO and controller design.

(ii) Different from most ESOs of the disturbance observer, the structure of an ESO is adjusted to estimate the states of the modified PMSM model as well as the ESN is adopted to approximate the unknown hysteretic losses. That not only guarantees the convergence of ESO fastly but also simplifies the observer design.

(iii) An SMC is designed with the designed ESO for this transformed PMSM model in electric vehicle systems and utilizes the continuous function $\tanh(\cdot)$ replacing the discontinuous function $\text{sign}(\cdot)$ to restrain the SMC chatting.

The rest of the paper is organized as follows: Section 2 discusses the problem formulations that give the new PMSM model and the transformation of the canonical form. The introduction of ESN is provided in Section 3, and Section 4 gives the ESO design, which includes the ESN, and the observer effectiveness is guaranteed. The neural network sliding mode control design is discussed in Section 5, and Section 6 shows simulations. Section 7 concludes this paper.

2. Problem Formulations

The electric vehicle model includes different sections, which is composed of vehicle derive, engine, motor, battery, rear and front wheels, and other electrical and mechanical accessory models. In this paper, we discuss the motor model of the vehicle with hysteresis nonlinearity. According to reference [40], the permanent magnet synchronous motor (PMSM) $d-q$ model can be described as follows:

$$\begin{cases} \dfrac{\mathrm{d}i_q}{\mathrm{d}t} = -\dfrac{R}{L_q}i_q + \dfrac{\omega L_d}{L_q}i_d - \dfrac{K_l}{L_q}\omega + \dfrac{1}{L_q}v_q, \\ \dfrac{\mathrm{d}i_d}{\mathrm{d}t} = -\dfrac{R}{L_d}i_d - \dfrac{\omega L_q}{L_d}i_q + \dfrac{1}{L_d}v_d, \\ T = K_t i_q + K_l\left(L_d - L_q\right)i_d i_q, \end{cases} \tag{1}$$

where i_d, i_q, v_d, and v_q represent the motor $d-q$-axes currents and voltages, respectively; R and L_d and L_q mean the motor resistance and $d-q$-axes inductances, respectively; K_l and K_t are the motor-induced voltage constant and motor torque constant, respectively; T is the transmit torque; and ω represents the motor speed.

From (1), it is obviously shown that the motor model parameters are viewed as constants. But it neglects hysteresis loss, cross coupling, eddy current loss, etc. In addition, according to the discussion of reference [40], since the number of rotor teeth is sufficiently high, one can assume that $L_d \approx L_q$. Then, considering the effect of the neglected factors in former models, especially the hysteresis loss, the model (1) is modified as

$$\begin{cases} \dfrac{\mathrm{d}i_q}{\mathrm{d}t} = -\dfrac{R}{L_q}i_q + \dfrac{\omega L_d}{L_q}i_d - \dfrac{K_l}{L_q}\omega + \dfrac{1}{L_q}v_q + f_1\left(i_q, i_d\right), \\ \dfrac{\mathrm{d}i_d}{\mathrm{d}t} = -\dfrac{R}{L_d}i_d - \dfrac{\omega L_q}{L_d}i_q + \dfrac{1}{L_d}v_d + f_2\left(i_q, i_d\right), \\ T \approx K_t i_q, \end{cases} \tag{2}$$

where $f_1(i_q, i_d)$, $f_2(i_q, i_d)$, and $g_1(i_q, i_d)$ are the unknown nonlinear smooth functions which represent the neglected factors such as hysteresis loss in (1). We rewrite the model (2) to the state-space form as follows:

$$\begin{cases} \dfrac{\mathrm{d}}{\mathrm{d}t}\underbrace{\begin{bmatrix} i_q \\ i_d \end{bmatrix}}_{x} = \underbrace{\begin{bmatrix} -\dfrac{R}{L_q} & \dfrac{\omega L_d}{L_q} \\ -\dfrac{\omega L_q}{L_d} & -\dfrac{R}{L_d} \end{bmatrix}}_{A}\begin{bmatrix} i_q \\ i_d \end{bmatrix} + \underbrace{\begin{bmatrix} \dfrac{1}{L_q} \\ \dfrac{1}{L_d} \end{bmatrix}}_{B}\begin{bmatrix} v_q \\ v_d \end{bmatrix} + \underbrace{\begin{bmatrix} f_1\left(i_q, i_d\right) \\ f_2\left(i_q, i_d\right) \end{bmatrix}}_{f(x)}, \\ \underbrace{\dfrac{T}{K_t}}_{y} = i_q, \end{cases} \tag{3}$$

where

$$x = \begin{bmatrix} x_1 \\ x_2 \end{bmatrix} = \begin{bmatrix} i_q \\ i_d \end{bmatrix},$$

$$A = \begin{bmatrix} a_{11} & a_{12} \\ a_{21} & a_{22} \end{bmatrix} = \begin{bmatrix} -\dfrac{R}{L_q} & \dfrac{\omega L_d}{L_q} \\ -\dfrac{\omega L_q}{L_d} & -\dfrac{R}{L_d} \end{bmatrix}, \tag{4}$$

$$B = \begin{bmatrix} b_1 \\ b_2 \end{bmatrix} = \begin{bmatrix} \dfrac{1}{L_q} \\ \dfrac{1}{L_d} \end{bmatrix} f(x) = \begin{bmatrix} f_1(x) \\ f_2(x) \end{bmatrix} = \begin{bmatrix} f_1(i_q, i_d) \\ f_2(i_q, i_d) \end{bmatrix}.$$

Many observers and controllers require that the system model should be in canonical form. To facilitate the observer and control design in this paper, a set of new state variables will be employed to transform the system model (2) into a canonical form. Define the new system states as

$$\begin{cases} z_1 = x_1, \\ z_2 = \dot{z}_1. \end{cases} \tag{5}$$

Then, according to the equation $z_2 = \dot{z}_1 = \dot{x}_1 = -(R/L_q)i_q + (\omega L_d/L_q)i_d - (K_l/L_q)\omega + (1/L_q)v_q + f_1(i_q, i_d)$, we have

$$\begin{aligned} \dot{z}_2 &= \ddot{z}_1 \\ &= -\frac{R}{L_q} z_2 + \frac{\omega L_d}{L_q}\left(-\frac{R}{L_d} i_d - \frac{\omega L_q}{L_d} i_q + \frac{1}{L_d} v_d + f_2(x)\right) + \dot{f}_1(x) \\ &= \underbrace{-\omega^2}_{\overline{a}_1} z_1 \underbrace{-\frac{R}{L_q}}_{\overline{a}_2} z_2 + \underbrace{\frac{\omega}{L_q}}_{\breve{b}} \underbrace{v_d}_{u} \underbrace{-\frac{\omega R}{L_q} i_d + \frac{\omega L_d}{L_q} f_2(x) + \dot{f}_1(x)}_{\overline{F}(x)}. \end{aligned} \tag{6}$$

In this paper, we adopt the Bouc–Wen hysteresis model to describe the hysteresis loss of the vehicle PMSM $d-q$ model. The Bouc–Wen model is given as follows:

$$\begin{aligned} f(x) &= \varsigma_1 u + \varsigma_2 \chi, \\ \dot{\chi} &= \varpi_0 \dot{u} - \varpi_1 |\dot{u}| |\chi|^{h-1} \chi - \varpi_2 \dot{u} |\chi|^h, \end{aligned} \tag{7}$$

where $\varpi_0 > 0, \varpi_1 > |\varpi_2|$, $h > 1, \chi(0) = 0$, and $\chi = [\chi_1, \chi_2]^T \in \mathbb{R}^2$.

Remark 1. At three-phase motor system, we have $v_d = \sqrt{(3/2)}U_m$, $v_q = 0$, where U_m represents the root-mean-square (RMS) value of the input voltage by coordinate transform. Then, without loss of generality, we assume $v_q = 0$ during the control process.

Then, equation (6) can be deduced as

$$\begin{aligned} \dot{z}_2 &= \overline{a}_1 z_1 + \overline{a}_2 z_2 + \breve{b} u - \frac{\omega R}{L_q} i_d + \frac{\omega L_d}{L_q}(\varsigma_{12} u + \varsigma_{22}\chi_2) + \varsigma_{11}\dot{u} + \varsigma_{21}\dot{\chi}_1 \\ &= \overline{a}_1 z_1 + \overline{a}_2 z_2 + \underbrace{\left(\breve{b} + \frac{\omega L_d \varsigma_{12}}{L_q}\right)}_{\overline{b}} u \underbrace{- \frac{\omega R}{L_q} i_d + \frac{\omega L_d}{L_q}\varsigma_{22}\chi_2 + \varsigma_{11}\dot{u} + \varsigma_{21}\dot{\chi}_1}_{F(x)}, \end{aligned} \tag{8}$$

where χ_1 and χ_2 are defined in (7).

Remark 2. The Bouc–Wen model is a mathematical model for hysteresis nonlinearity, where the parameters ς_1 and ς_2 decide the direction of the hysteresis nonlinearity. If $\varpi_0 = 2, \varpi_1 = 4, \varpi_2 = 0.5, h = 3, \varsigma_1 = 3$, and $\varsigma_2 = 5$, the input signal $u = 2.5\sin(1.5\pi)$; then, the curve of the Bouc–Wen model is illustrated in Figure 1. If the parameters $\varsigma_1 = -3$ and $\varsigma_2 = -5$ and other parameters are not changed, the curve is illustrated in Figure 2. It is obviously shown that the parameters ς_1 and ς_2 decide the direction of the Bouc–Wen model.

Then, the system model is transformed into the canonical form as

$$\begin{cases} \dot{z}_1 = z_2, \\ \dot{z}_2 = \overline{a}_1 z_1 + \overline{a}_2 z_2 + \overline{b} u + F(x), \\ y = z_1. \end{cases} \tag{9}$$

3. Echo State Network

The echo state network (ESN) is relatively a new recurrent neural network (RNN) structure for complex dynamical systems. The structure of ESN is composed of a dynamical recursive hidden layer and a memoryless output layer. Because of the feedback recursive hidden layers like the echoes, the structure of the neural network is named ESN.

ESN has easily supervised training. Compared with some other NNs, the ESN can fastly, simply, and constructively realize the supervised learning. In addition, without changing all the weights between the input layer and hidden layer, only by changing the weights from the reservoir to the output layer, ESN can fastly obtain higher precision.

The continuous-time leaky integrator ESN can be defined as

$$\dot{\Omega} = \alpha(-\gamma\Omega + \psi(W_{\text{in}}\nu + W_{\text{it}}\Omega + W_{\text{ba}}\xi)), \tag{10}$$

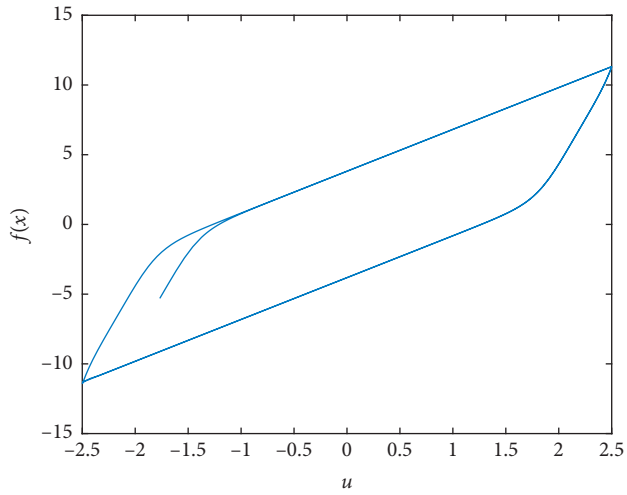

FIGURE 1: The curve of the Bouc–Wen model with $\varsigma_1 = 3$ and $\varsigma_2 = 5$.

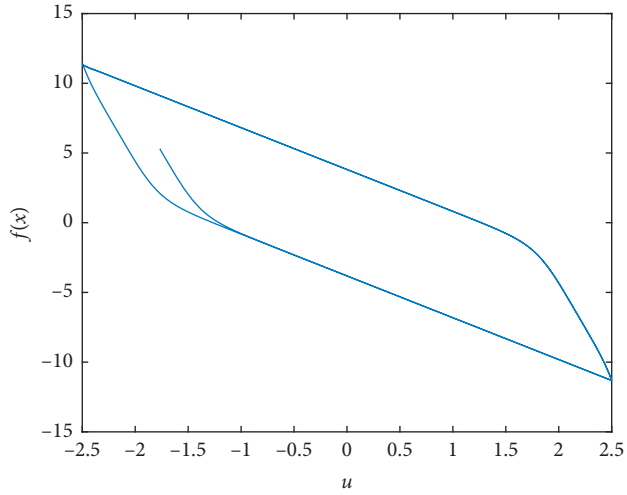

FIGURE 2: The curve of the Bouc–Wen model with $\varsigma_1 = -3$ and $\varsigma_2 = -5$.

where Ω represents the n-dimensional dynamic state; $\alpha > 0$ is a time constant; γ is the leaking decay rate of the neuron's set Ω; ψ represents a given real continuous function, in this paper, we chose the Gaussian function; and $W_{\text{in}} \in \mathbb{R}^{n\times m}, W_{\text{it}} \in \mathbb{R}^{n\times n}$, and $W_{\text{ba}} \in \mathbb{R}^{n\times m}$ are the input, internal, and feedback weight matrices, respectively.

As suggested in [29], by choosing $\alpha = 1$ and $\gamma = 1$, equation (10) is rewritten as

$$\dot{\Omega} = -\Omega + \psi\left(W_{\text{in}}\nu + W_{\text{it}}\Omega + W_{\text{ba}}\xi\right). \tag{11}$$

Then, the kernel function is chosen as the Gaussian function and Ω is defined as $\Omega(x) = [s_1(x), s_2(x), \ldots, s_l(x)]$ with l the neuron node number of the ESN output layer. The function is

$$s_i(x) = \exp\left\{-\frac{(x-\varrho_i)^T(x-\varrho_i)}{\rho^2}\right\}, \tag{12}$$

where $\varrho_i = [\varrho_{i1}, \varrho_{i2}, \ldots, \varrho_{iq}]^T$, $i = 1, 2, \ldots, l$; q means the input number; and ρ represents the width of the Gaussian function.

Defining the output activation function Θ is chosen as, the output of ESN is defined as

$$\Gamma = \Theta(W\Omega). \tag{13}$$

According to the literature [29], the output activation function Θ units had no memory so that their values at time $i+1$ depended only fractionally and indirectly on their previous values. Thus, those networks are best suited for modeling intrinsically discrete-time systems with a computational and jumpy flavor. It is difficult to use networks with continuous dynamics. But we can define the ESNs with continuous function so that the dynamics can be approximated by this continuous function.

For any given real continuous function $G(\cdot)$: $\mathbb{R}^n \longrightarrow \mathbb{R}$ on a sufficiently large compact set Ξ and arbitrary ε_M, the ESN system Γ satisfies

$$\sup_{\Omega\in\Xi} \|G - \Gamma\| \le \varepsilon_M, \tag{14}$$

where G is a given real continuous function on a sufficiently large compact set $\Xi \subset \mathbb{R}$ with the supremum $\varepsilon_M > 0$.

Then, the function G can be expressed as

$$G = W^*\Omega(x) + \varepsilon^*, \tag{15}$$

where $\varepsilon^* \le \varepsilon_M$ is the ESN error.

4. Extended State Observer Design

Since the nonlinearities including hysteresis loss are considered, the controller cannot be directly designed, and the system states need an observer. Considering the normalized form (9), we will design an extended state observer (ESO) to approximate the system states. Before designing the ESO, an extended state z_3 will be defined and the extended state system model is expressed as follows:

$$\begin{cases} \dot{z}_1 = z_2, \\ \dot{z}_2 = z_3 + \overline{b}u, \\ \dot{z}_3 = \overline{a}_1 z_1 + \overline{a}_2 z_2 + F(x). \end{cases} \tag{16}$$

Then, the ESO is designed as

$$\begin{cases} \dot{\widehat{z}}_1 = \widehat{z}_2 + \beta_1(y - \widehat{z}_1), \\ \dot{\widehat{z}}_2 = \widehat{z}_3 + \overline{b}u + \beta_2(y - \widehat{z}_1), \\ \dot{\widehat{z}}_3 = \overline{a}_1\widehat{z}_1 + \overline{a}_2\widehat{z}_2 + \widehat{F}(x) + \beta_3(y - \widehat{z}_1), \end{cases} \tag{17}$$

where $\widehat{z}_1, \widehat{z}_2, \widehat{z}_3$, and $\widehat{F}(x)$ are the estimations of z_1, z_2, z_3, and $F(x)$, respectively, and β_1, β_2, and β_3 are the designed high gain parameters, respectively.

Define the errors

$$\begin{cases} \widetilde{z}_i = z_i - \widehat{z}, \quad i = 1, 2, 3, \\ \widetilde{y} = y - \widehat{y}, \\ \widetilde{F}(x) = F(x) - \widehat{F}(x), \end{cases} \tag{18}$$

where $F(x)$ is described by the ESN. Therefore, it has $F(x) = W\Omega(x) + \varepsilon$ and $\widehat{F}(x) = \widehat{W}\Omega(x)$. Then, we have $\widetilde{F}(x) = \widetilde{W}\Omega(x) + \varepsilon = W\Omega(x) + \varepsilon - \widehat{W}\Omega(x)$, and define the update law of $\widetilde{W}$ as

$$\dot{\widetilde{W}} = \dot{\widehat{W}} = U(\widehat{e}\Omega(x) - \varepsilon|\widehat{e}|\widehat{W}), \tag{19}$$

where $U = U^T$ is a constant matrix, ϵ is a designed positive constant, and $\widehat{e}$ is defined in (36).

Lemma 1. *[41] The ESN weights $\widehat{W}$ in equation (19) are bounded by $\|\widehat{W}\| \le \|\varpi\|_M/\epsilon$, where $\|\varpi\|_M$ is the bound of the ESN basis function vector, i.e., $\|\Omega\| \le \|\varpi\|_M$.*

Proof. From the previous discussion, the ESN basis function vector Ω are Gaussian functions so that it is bounded obviously, i.e., $\|\Omega\| \le \|\varpi\|_M$. We choose the Lyapunov function candidate as

$$V_N = \frac{1}{2U}\widehat{W}^T\widehat{W}, \tag{20}$$

and then, considering equation (19), the time derivative of V_N can be deduced as

$$\begin{aligned}\dot{V}_N &= \frac{1}{U}\widehat{W}^T\dot{\widehat{W}}\\ &= \widehat{W}^T(\widehat{e}\Omega(x) - \varepsilon|\widehat{e}|\widehat{W})\\ &\le -\|\widehat{W}\||\widehat{e}|\left(\varepsilon\|\widehat{W}\| - \|\varpi\|_M\right).\end{aligned} \tag{21}$$

According to reference [41], $\widehat{W}$ is bounded by $\|\widehat{W}\| \le \|\varpi\|_M/\epsilon$ and thus $\widetilde{W} = W^* - \widehat{W}$ is also bounded as $\|\widetilde{W}\| \le \|\omega\|_M$, where $\|\omega\|_M = W_N + (\|\varpi\|_M/\epsilon)$.

Then, considering (16) and (17) yields

$$\begin{cases}\dot{\widetilde{z}}_1 = -\beta_1\widetilde{z}_1 + \widetilde{z}_2,\\ \dot{\widetilde{z}}_2 = -\beta_2\widetilde{z}_1 + \widetilde{z}_3,\\ \dot{\widetilde{z}}_3 = (\overline{a}_1 - \beta_2)\widetilde{z}_1 + \overline{a}_2\widetilde{z}_2 + \widetilde{F}(x).\end{cases} \tag{22}$$

Equation (22) can be rewritten as

$$\dot{\widetilde{z}} = \overline{A}\widetilde{z} + \zeta\widetilde{F}(x), \tag{23}$$

where

$$\begin{aligned}\overline{A} &= \begin{bmatrix}-\beta_1 & 1 & 0\\ -\beta_2 & 0 & 1\\ \overline{a}_1 - \beta_3 & \overline{a}_2 & 0\end{bmatrix},\\ \zeta &= \begin{bmatrix}0\\0\\1\end{bmatrix}.\end{aligned} \tag{24}$$

Considering that the high gain parameters β_1, β_2, and β_3 are designed, the characteristic polynomial of $\overline{A}$ is Hurwitz. Then, given a positive definite symmetric matrix $P = P^T > 0$, the existing positive definite symmetric matrix $Q = Q^T > 0$ satisfies

$$\overline{A}^T P + P\overline{A} \le -Q. \tag{25}$$

□

Remark 3. In most cases, ESO has been utilized to estimate the generalized disturbance. But in this paper, the structure of the ESO has been adjusted to approximate the system states. If appropriate high gains β_1, β_2, and β_3 are chosen, the ESO can fastly and precisely estimate the states. Besides, adjusting ESO can easily guarantee the convergence of the observer.

Therefore, the following theorem holds.

Theorem 1. *Considering the vehicle drive PMSM model (2), which is transformed into canonical form (9), the unknown nonlinearity $F(x)$ is approximated by an ESN (15), the normalized system (9) is extended to (16), and then, all the signals are bounded and the states can be observed by an ESO (17).*

Proof. Considering the ESO (17) and equation (22), the Lyapunov function candidate V_o for the state observer errors can be designed as

$$V_o = \widetilde{z}^T P\widetilde{z}. \tag{26}$$

Considering (15), the derivative of V_o is deduced as

$$\begin{aligned}\dot{V}_o &= \widetilde{z}^T\left(\overline{A}^T P + P\overline{A}\right)\widetilde{z} + 2\widetilde{F}(x)\zeta^T P\widetilde{z}\\ &\le -\widetilde{z}^T Q\widetilde{z} + 2\widetilde{W}\Omega(x)P\widetilde{z} + 2\varepsilon,\end{aligned} \tag{27}$$

where $\widetilde{W} = W - \widehat{W}$ and $\widehat{W}$ is the estimation of the ESN weight, and the unknown nonlinearity $F(x)$ is approximated by ESN $F(x) = W\Omega(x) + \varepsilon$; therefore, the estimation $\widehat{F}(x)$ is $\widehat{F}(x) = \widehat{W}\Omega(x)$.

According to Lemma 1 and reference [31], the error weight of ESN satisfies $\widetilde{W} \le \|w\|_M$, and $\Omega(x)$ is bounded, it has $\Omega(x) \le \|\varpi\|_M$. Considering $\varepsilon \le \varepsilon_M$, equation (27) is expressed as

$$\begin{aligned}\dot{V}_o &\le -\widetilde{z}^T Q\widetilde{z} + 2\|w_M\varphi_M\|\lambda_{\max}(P)\widetilde{z} + 2\varepsilon_M\\ &\le -\widetilde{z}^T Q\widetilde{z} + 2\|w_M\|\|\varphi_M\|\lambda_{\max}(P)\widetilde{z} + 2\varepsilon_M,\end{aligned} \tag{28}$$

where $\lambda_{\max}(P)$ represents the biggest norm of the matrix P. From Young's inequality $ab \le ((a^2 + b^2)/2)$, it has $2\|w_M\|\|\varphi_M\|\lambda_{\max}(P)\widetilde{z} \le \|w_M\|^2 + \|\varphi\|^2 + \lambda^2_{\max}(P) + \widetilde{z}^2$. Then, we have

$$\dot{V}_o \le -\widetilde{z}^T Q\widetilde{z} + \|w_M\|^2 + \|\varphi\|^2 + \lambda^2_{\max}(P) + \widetilde{z}^2 + 2\varepsilon_M. \tag{29}$$

We rewrite (29) as

$$\dot{V}_o \le -\breve{a}_1 V_o + \breve{a}_2, \tag{30}$$

where $\breve{a}$ can be deduced by $\overline{A}^T P + P\overline{A} \le -Q$; $\breve{a}_2 = \|w_M\|^2 + \|\varphi\|^2 + \lambda^2_{\max}(P) + \widetilde{z}^2 + 2\varepsilon_M$. By integrating both sides of (30), the following equation can be obtained:

$$|\widetilde{z}| \le \sqrt{\frac{V_o(0)e^{-\breve{a}_1 t} + \left(\breve{a}_2/\breve{a}_1\right)}{\lambda_{\max}(P)}}, \tag{31}$$

and that indicates all the signals are bounded and the observer error $\tilde{z}$ is converged into a compact set around the zero. Therefore, according to the Lyapunov theory, the proposed ESO can estimate the system states. □

5. Sliding Mode Control Design

This section will design a sliding mode control for the new vehicle drive PMSM model that the hysteresis loss is described by ESN. The control structure of the sliding mode control with the ESO and ESN is illustrated in Figure 3. We firstly define a sliding mode manifold and then design the sliding mode controller. The stability of the control strategy finally is demonstrated.

To design the sliding mode control, the tracking error is defined as

$$e = y - y_d = z_1 - y_d, \tag{32}$$

and the sliding manifold is adopted as

$$s = \eta e + \dot{e}, \tag{33}$$

where the designed parameters $\eta > 0$ and the reference signal y_d has continual derivative.

From (32), the derivative of s can be deduced as

$$\dot{s} = \eta \dot{e} + \ddot{e}. \tag{34}$$

Because the tracking error is defined in (32), we have

$$\begin{aligned} \dot{e} &= \dot{z}_1 - \dot{y}_d = z_2 - \dot{y}_d, \\ \ddot{e} &= \dot{z}_2 - \ddot{y}_d. \end{aligned} \tag{35}$$

We define the functions as

$$\begin{aligned} \hat{e} &= \hat{y} - y_d = \hat{z}_1 - y_d, \\ \hat{s} &= \eta \hat{e} + \dot{\hat{e}}, \\ \tilde{s} &= s - \hat{s}, \\ \tilde{e} &= e - \hat{e}. \end{aligned} \tag{36}$$

The sliding mode controller is designed as

$$u = \frac{1}{\overline{b}}\left(-\eta_t \hat{s} - \hat{z}_3 - \eta \dot{\hat{e}} + \ddot{y}_d - \tau \operatorname{sign}(s)\right), \tag{37}$$

where the designed parameters $\eta_t > 0$ and $\hat{s}$ and $\hat{e}$ represent the estimation of s and e, respectively. In order to decrease the influence of the chattering, we choose $0 < \tau < 1$.

Then, the following theorem can be obtained:

Theorem 2. *For the vehicle drive PMSM model considering the hysteresis loss (9), which extends the state to (16), the states are observed by ESO (17); defining the sliding mode manifold in (33) and designing the controller in (37), then, all signals in the closed-loop are uniformly ultimately bounded (UUB).*

Proof. To verify the stability of the closed loop, the Lyapunov function is selected as

$$V = \frac{1}{2}s^2. \tag{38}$$

Considering the sliding manifold (33)–(35), the derivative of V is

$$\begin{aligned} \dot{V} &= s\dot{s} \\ &= s(\eta \dot{e} + \ddot{e}) \\ &= s(\eta \dot{e} + (\dot{z}_2 - \ddot{y}_d)). \end{aligned} \tag{39}$$

Substituting $\dot{z}_2 = z_3 + \overline{b}u$ in (16) into (39) yields

$$\dot{V} = s\left(\eta \dot{e} + \left(z_3 + \overline{b}u - \ddot{y}_d\right)\right). \tag{40}$$

By the substitution of sliding mode controller (37) into (40), the derivative of V can be deduced as

$$\dot{V} = s\left(\eta \dot{e} + \left(z_3 - \eta_t \hat{s} - \hat{z}_3 - \eta \dot{\hat{e}} + \ddot{y}_d - \tau \operatorname{sign}(s) - \ddot{y}_d\right)\right). \tag{41}$$

Considering (36), the derivative of V can be deduced as

$$\begin{aligned} \dot{V} &= s\left(\eta \dot{\tilde{e}} + \tilde{z}_3 - \eta_t \hat{s} - \tau \operatorname{sign}(s)\right) \\ &= s\left(\eta \dot{\tilde{e}} + \tilde{z}_3 - \eta_t (s - \tilde{s}) - \tau \operatorname{sign}(s)\right) \\ &= -\eta_t s^2 + s\left(\eta \dot{\tilde{e}} + \tilde{z}_3 + \eta_t \tilde{s} - \tau \operatorname{sign}(s)\right). \end{aligned} \tag{42}$$

Substituting the sliding manifold (33) and $\hat{s} = \eta \hat{e} + \dot{\hat{e}}$ in (36) into $\tilde{s}$ yields

$$\tilde{s} = \eta \tilde{e} + \dot{\tilde{e}}. \tag{43}$$

By the substitution of (43) into (42), we get

$$\begin{aligned} \dot{V} &= -\eta_t s^2 + s\left(\eta \dot{\tilde{e}} + \tilde{z}_3 + \eta \eta_t \tilde{e} + \eta_t \dot{\tilde{e}} - \tau \operatorname{sign}(s)\right) \\ &= -\eta_t s^2 + s\left((\eta + \eta_t)\dot{\tilde{e}} + \tilde{z}_3 + \eta \eta_t \tilde{e} - \tau \operatorname{sign}(s)\right). \end{aligned} \tag{44}$$

According to $e = z_1 - y_d$ in (32), we have

$$\begin{aligned} \tilde{e} &= \tilde{z}_1 - y_d, \\ \dot{\tilde{e}} &= \tilde{z}_2 - \dot{y}_d. \end{aligned} \tag{45}$$

Substituting (22) and (45) into (44) yields

$$\begin{aligned} \dot{V} &= -\eta_t s^2 + s\left((\eta + \eta_t)\tilde{z}_2 - (\eta + \eta_t)\dot{y}_d + \overline{a}_1 \tilde{z}_1 + \overline{a}_2 \tilde{z}_2 + \tilde{F}(x) + \eta \eta_t \tilde{z}_1 - \eta \eta_t y_d - \tau \operatorname{sign}(s)\right) \\ &= -\eta_t s^2 + s\left((\overline{a}_1 + \eta \eta_t)\tilde{z}_1 + (\overline{a}_2 + \eta + \eta_t)\tilde{z}_2 - \eta \eta_t y_d - (\eta + \eta_t)\dot{y}_d + \tilde{F}(x) - \tau \operatorname{sign}(s)\right). \end{aligned} \tag{46}$$

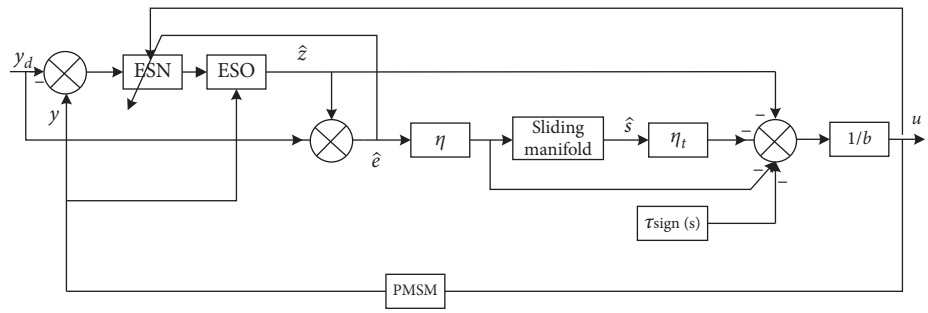

Figure 3: The structure of the controller.

Considering Theorem 1, the unknown bounded function $\widetilde{F}(x)$ can be approximated by the ESN $\widetilde{F}(x) = \widetilde{W}\Omega(x) \le \|\omega_M\|\|\varphi_M\|$ and $\widetilde{z}_1, \widetilde{z}_2, y_d$, and $\dot{y}_d$ are all bounded, respectively. Then, defining $\|(\overline{a}_1 + \eta\eta_t)\widetilde{z}_1 + (\overline{a}_2 + \eta + \eta_t)\widetilde{z}_2 - \eta\eta_t y_d - (\eta + \eta_t)\dot{y}_d + \widetilde{W}\Omega(x)\| \le \Delta_{\max}$, where $\Delta_{\max} \ge 0$, equation (46) satisfies

$$\begin{aligned} \dot{V} &\le -\eta_t s^2 + s\Delta_{\max} - \tau s\,\mathrm{sign}(s) \\ &\le -\eta_t s^2 + s\Delta_{\max} - \tau|s|. \end{aligned} \tag{47}$$

If $\tau|s| > 1$, equation (47) can be rewritten as

$$\begin{aligned} \dot{V} &\le -\eta_t s^2 + s\Delta_{\max} \\ &= -\mu + s\Delta_{\max}, \end{aligned} \tag{48}$$

where $\mu = \eta_t > 0$.

If $0 \le \tau|s| \le 1$, it has

$$\begin{aligned} \dot{V} &\le -\eta_t s^2 + s\Delta_{\max} - \tau s^2 \\ &= -(\eta_t + \tau)s^2 + s\Delta_{\max} \\ &= -\mu s^2 + s\Delta_{\max}, \end{aligned} \tag{49}$$

where $\mu = \eta_t + \tau > 0$.

According to Young's inequality, $s\Delta_{\max}$ has $s\Delta_{\max} \le (s^2/2) + (\Delta_{\max}^2/2)$; then, equation (47) can be rewritten as

$$\begin{aligned} \dot{V} &\le -\mu s^2 + \frac{s^2}{2} + \frac{\Delta_{\max}^2}{2} \\ &= \left(-\mu + \frac{1}{2}\right)s^2 + \frac{\Delta_{\max}^2}{2}. \end{aligned} \tag{50}$$

When $\mu > 0.5$, according to the definition of the Lyapunov function V in (38), equation (50) can be solved

$$|s| \le \sqrt{\frac{(2\mu - 1)V(0) + \Delta_{\max}^2}{(2\mu - 1)\Delta_{\max}}}. \tag{51}$$

Considering the definition of s in (33) and the bounded (51), the margin of error e is obtained:

$$|e| \le \sqrt{\frac{s(0) + (\eta/\vartheta)}{\vartheta}}, \tag{52}$$

where $\vartheta = \sqrt{((2\mu - 1)V(0) + \Delta_{\max}^2)/((2\mu - 1)\Delta_{\max})}$.

Therefore, according to the Lyapunov theory, all the signals of the closed loop are uniformly ultimately bounded. □

Remark 4. In this controller design, we chose the robust function sign$(\cdot)$ to design the sliding mode control. But the function sign$(\cdot)$ is a discontinuous function which can deduce the strong chattering for the sliding mode manifold. In order to restrain the chattering, many approaches are utilized. In this paper, we select the continuous function tanh$(\cdot)$ instead of the discontinuous function sign$(\cdot)$, which can substantially restrain the chattering of the SMC. The simulations are demonstrated for this approach.

6. Simulations

We design the simulations with Simulink of Matlab to verify the effectiveness of the proposed ESO and ESNSMC for the vehicle drive motor with hysteresis nonlinearity. The PMSM, the ESO, and the ESNSMC parameters are selected as follows:d – axis inductance L_d and q – axis inductance L_q are 0.47 mH; torque T is 96.5 N · m; angular speed ω is 3000 rpm; resistance R is 0.033 Ω; motor-induced voltage constant K_l is 0.147; and motor torque constant K_t is 0.72. The high gain parameters β_1, β_2, and β_3 are selected as $\beta_1 = 360$, $\beta_2 = 5000$, and $\beta_3 = 28500$. η is chosen as 5. τ can be selected as 0.3. In order to verify the proposed approaches, we restrain the errors in $[-0.5, 0.5]$ in the simulations.

In the section, we design two series of simulations with different values of τsign(s). One is τsign$(s) = 0.3$sign(s), and the other is selected as τsign$(s) = 0.3\tanh(s)$. The reason of the design is to contrast the results of the ESNSMC to show the effect of the chattering in the sliding mode control.

6.1. Case 1. In this section, we select τsign$(s) = 0.3$sign(s) in the controller of (37) to verify the proposed ESNSMC and ESO of this paper. The output tracking results of y, $\dot{y}$, and $\ddot{y}$ are illustrated in Figure 4, and the tracking errors are shown in Figure 5. The observer results of z_1, z_2, and z_3 of the proposed ESO are shown in Figure 6, and the observer errors are illustrated in Figure 7. Figure 8 is the proposed ESNSMC controller trajectory.

From Figures 4 and 6, it is obviously shown that both the proposed ESO and the ESNSMC are well tracking the reference signals. Based on the structure of the control strategy, the adjusting of the observer is in the closed loop and that follow the adjustment of the controller. Then, if the gains of ESO β_1, β_2, and β_3 are chosen enough higher, it can quickly approximate the states z_1, z_2, and z_3. From Figure 6, one can clearly find that the proposed ESO worked well, and from

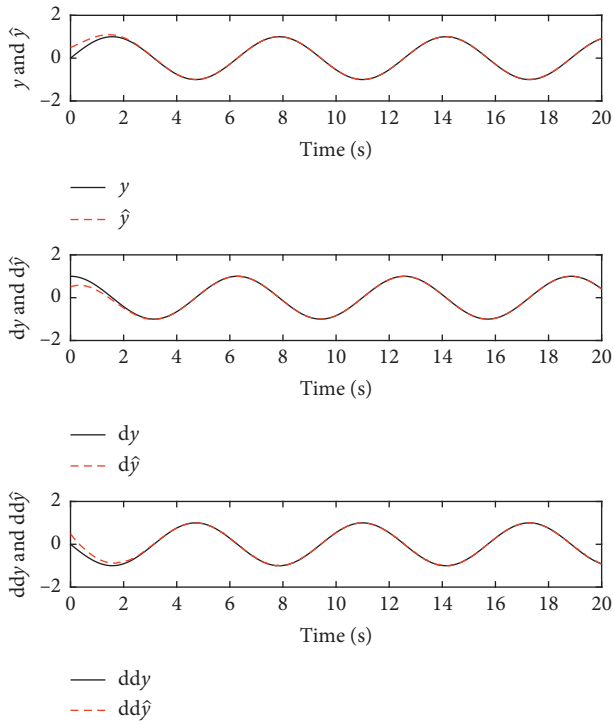

Figure 4: The output results $y, \mathrm{d}y$, and $\mathrm{dd}y$ of the ESNSMC with ESO $\tau\mathrm{sign}(s) = 0.3\mathrm{sign}(s)$.

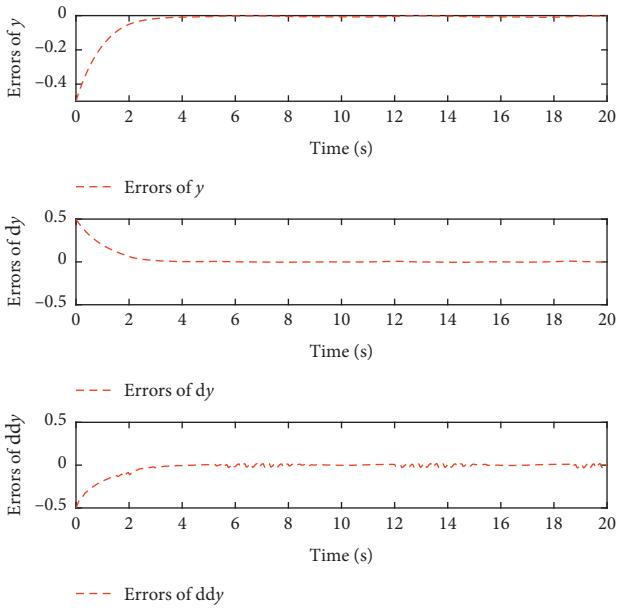

Figure 5: The errors of $y, \mathrm{d}y$, and $\mathrm{dd}y$ of the ESNSMC with ESO $\tau\mathrm{sign}(s) = 0.3\mathrm{sign}(s)$.

Figure 4, one can also find that the output quickly tracks the reference signal. But from Figures 5 and 7, due to the existence of the chattering in the sliding mode control, it has been obviously shaking when the PMSM is veered. If we survey Figure 8, it can be seen that the trajectory of the proposed ESMSMC controller also has the same characteristics as well as the errors of ESNSMC control results and the ESO observer.

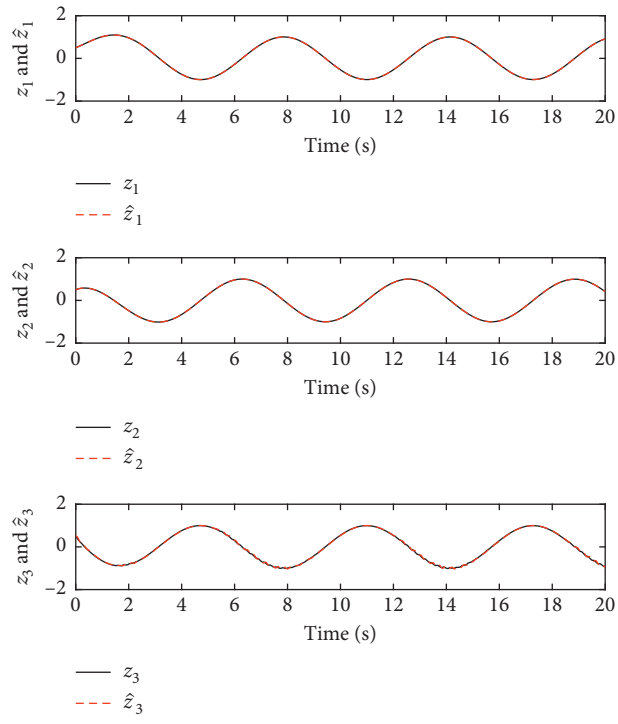

Figure 6: The observer results of z_1, z_2, and z_3 with ESO $\tau\mathrm{sign}(s) = 0.3\mathrm{sign}(s)$.

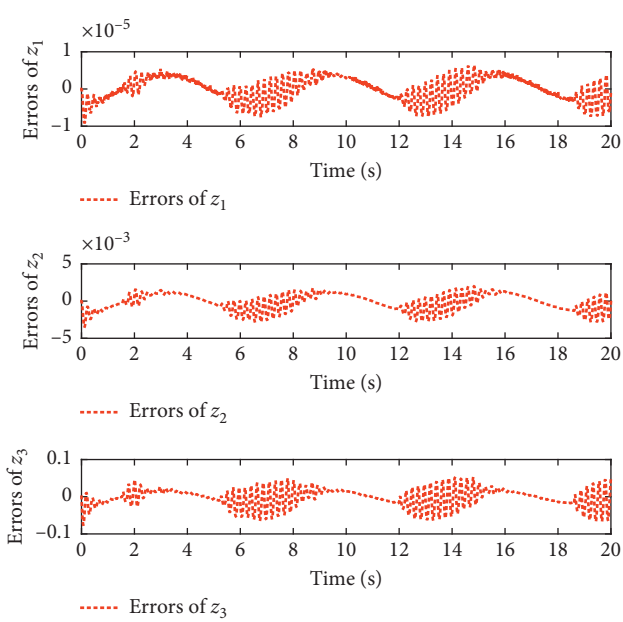

Figure 7: The observer errors of z_1, z_2, and z_3 with ESO $\tau\mathrm{sign}(s) = 0.3\mathrm{sign}(s)$.

From Figures 4–8, one can easily find the influence of the chattering in the proposed ESNSMC, even though the ESN compensates the hysteresis nonlinearity. The chattering of the sliding mode control really degrades the precision of the control strategy. In order to alleviate the influence of the chattering of the ESNSMC, we chose continuous $\tanh(\cdot)$ function to take the place of the discontinuous $\mathrm{sign}(\cdot)$ function in the next case.

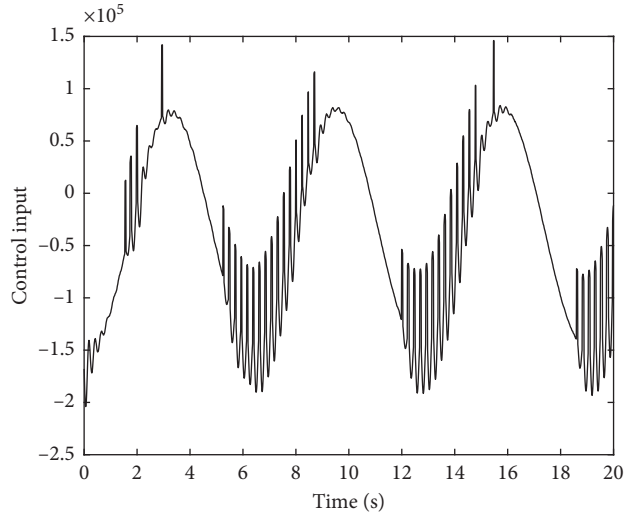

Figure 8: The trajectory of the ESNSMC controller $\tau\text{sign}(s) = 0.3\text{sign}(s)$.

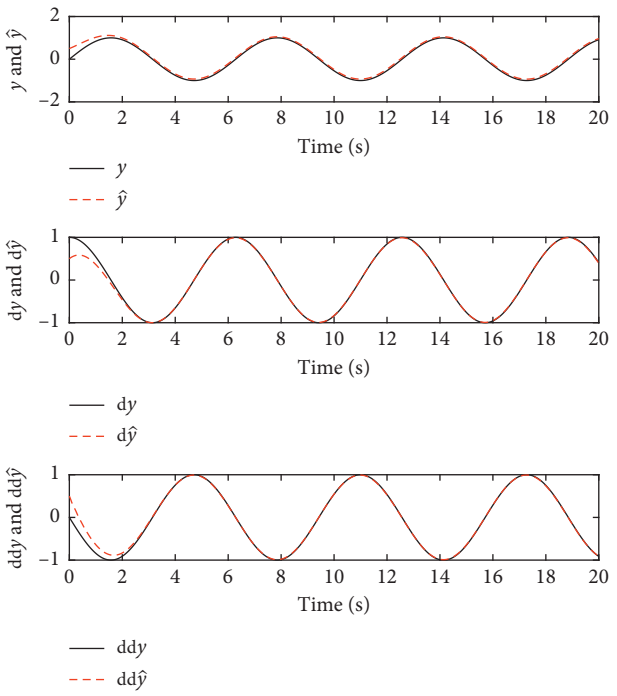

Figure 9: The output results $y, \mathrm{d}y$, and $\mathrm{dd}y$ of the ESNSMC with ESO $\tau\text{sign}(s)$ is replaced by $0.3\tanh(s)$.

6.2. Case 2. In this section, the robust $\tau\text{sign}(s)$ is chosen as $\tau\text{sign}(s) = 0.3\tanh(s)$. Then, Figures 9 and 10 illustrate the output results $y, \dot{y}$, and $\ddot{y}$ of the proposed ESNSMC with ESO for $\tau\text{sign}(s) = 0.3\tanh(s)$, and the ESO estimates the states z_1, z_2, and z_3 are shown in Figure 11. Figure 12 is the estimate errors of z_1, z_2, and z_3 with the ESO observer. The controller input is illustrated in Figure 13 for the robust $\tau\text{sign}(s) = 0.3\tanh(s)$.

Compared with the control tracking results Figures 4 and 9 and the controller errors Figures 5 and 10, one can obtained that the continuous function $\tanh(\cdot)$ can substantially restrain

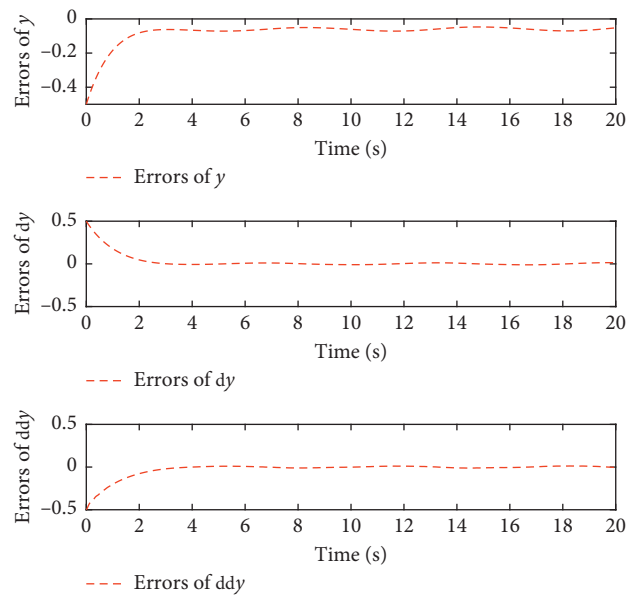

Figure 10: The errors of $y, \mathrm{d}y$, and $\mathrm{dd}y$ of the ESNSMC with ESO $\tau\text{sign}(s)$ is replaced by $0.3\tanh(s)$.

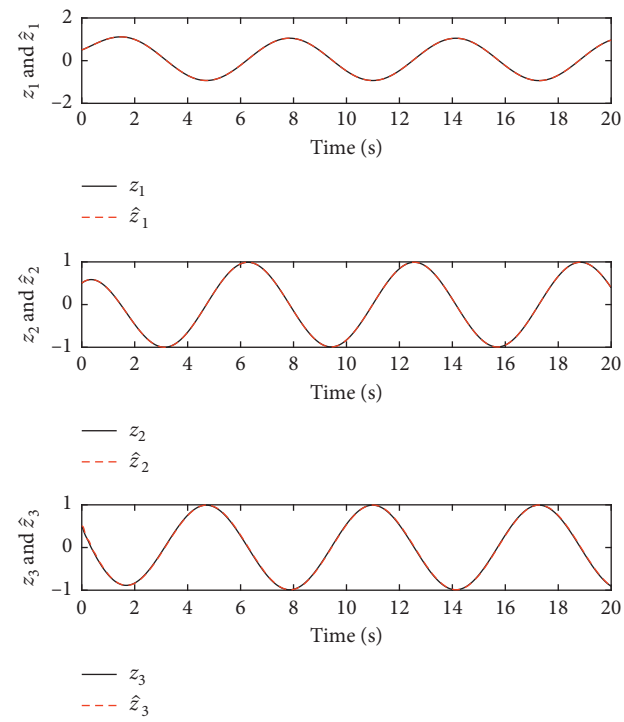

Figure 11: The observer results of z_1, z_2, and z_3 with ESO $\tau\text{sign}(s)$ is replaced by $0.3\tanh(s)$.

the chattering of the sliding mode control. Especially in contrast with the tracking errors Figures 5 and 10, the influence of the chattering at the reversing processes almost is not catched in Figure 10 with the continuous robust function $\tau\text{sign}(s) = 0.3\tanh(s)$. The same conclusions can also be deduced by the observer results and errors in Figures 11 and 12. Especially in contrast with Figures 7 and 12, one can find that the maximum of the error of z_3 is about 0.08 at the

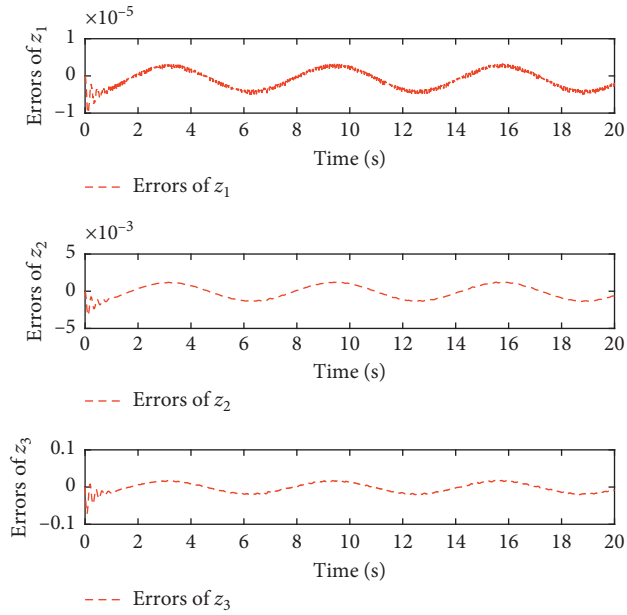

Figure 12: The observer errors of z_1, z_2, and z_3 with ESO $\tau \text{sign}(s)$ is replaced by $0.3\tanh(s)$.

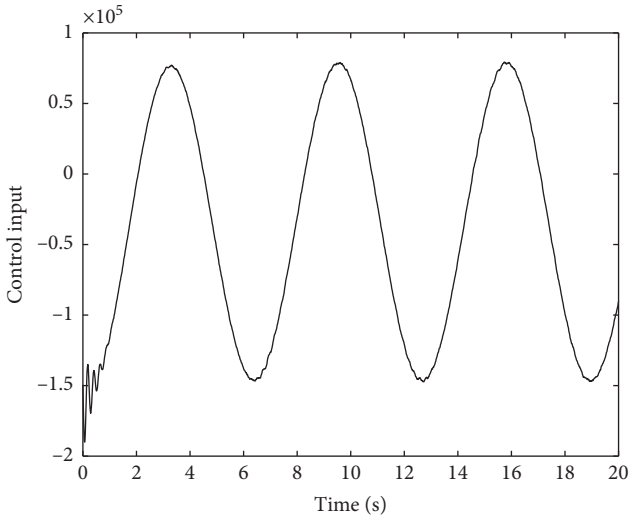

Figure 13: The trajectory of the ESNSMC controller $\tau \text{sign}(s)$ is replaced by $0.3\tanh(s)$.

reversing processes in Figure 7 and the maximum of the error of z_3 is about 0.02 at the reversing processes in Figure 12. One can also obtain that, in Figure 12, the maximum of errors of z_1, z_2, and z_3 appears at the dynamic processes with the continuous robust function $\tau \text{sign}(s) = 0.3\tanh(s)$, which are caused by the ESN, but in Figure 8, the maximum of errors of z_1, z_2, and z_3 appears at the reversing processes with discontinuous robust function $\tau \text{sign}(s) = 0.3\text{sign}(s)$, which are caused by the chattering of the SMC.

Table 1 illustrates the tracking errors and the observer errors with the discontinuous robust function $\tau \text{sign}(s) = 0.3\text{sign}(s)$, and the tracking errors and the observer errors with the continuous robust function $\tau \text{sign}(s) = 0.3\tanh(s)$ are shown in Table 2. From Tables 1 and 2, the MAEs of $[\tilde{z}_1, \tilde{z}_2, \tilde{z}_3]^T$ are $[2.702e^{-6}, 9.5797e^{-4}, 0.0187]^T$ and $[2.289e^{-6}, 8.3078e^{-4}, 0.0116]$, respectively. It is illustrated that the continuous robust function $\tanh(\cdot)$ can substantially restrain the chattering of the SMC. But considering the MAE tracking errors $[\tilde{y}, \dot{\tilde{y}}, \ddot{\tilde{y}}]^T$ are $[0.0276, 0.0269, 0.0317]^T$ and $[0.0775, 0.0281, 0.0312]^T$, respectively, the MIN tracking errors are $[0.0014, 1.8734e^{-6}, 1.3852e^{-5}]$ and $[0.047, 7.9464e^{-6}, 1.473e^{-5}]$, respectively. That means the continuous robust function $\tanh(\cdot)$ can substantially restrain the chattering but degrade the tracking precision.

Table 1: The tracking errors and the observer errors with the robust $\tau \text{sign}(s) = 0.3\text{sign}(s)$

Variables	MAE	Max	Min
$\tilde{y}$	0.0276	0.5	0.0014
$\dot{\tilde{y}}$	0.0269	0.5	$1.8734e^{-6}$
$\ddot{\tilde{y}}$	0.0317	0.5	$1.3852e^{-6}$
$\tilde{z}_1$	$2.702e^{-6}$	$9.9556e^{-6}$	0
$\tilde{z}_2$	$9.5797e^{-4}$	0.0035	0
$\tilde{z}_3$	0.0187	0.0763	0

Table 2: The tracking errors and the observer errors with the robust $\tau \text{sign}(s) = 0.3\tanh(s)$.

Variables	MAE	Max	Min
$\tilde{y}$	0.0775	0.5	0.047
$\dot{\tilde{y}}$	0.0281	0.5	$7.9464e^{-6}$
$\ddot{\tilde{y}}$	0.0312	0.5	$1.473e^{-5}$
$\tilde{z}_1$	$2.2891e^{-6}$	$8.3371e^{-6}$	0
$\tilde{z}_2$	$8.3078e^{-4}$	0.0032	0
$\tilde{z}_3$	0.0116	0.0698	0

Compared with Figures 8 and 13, one can obviously find that the dynamic processes is influenced by the ESN in Figure 13 with the continuous robust function $\tanh(\cdot)$ which can well restrain the chattering of the SMC, but the discontinuous robust function $\text{sign}(\cdot)$ will result in strong chattering and difficult to achieve stable process from Figure 8.

7. Conclusion

A new neural network sliding mode control strategy was designed for PMSM of electric vehicles in this research. Firstly, a modified PMSM model considering hysteresis losses was proposed. Since the existence of the hysteresis nonlinearity complicated the PMSM model, a transformed canonical form was deduced to simplify the controller. Because most electric vehicle system states could not be measured directly, an ESO was adopted to estimate all the states including the indirectly obtained states, and the hysteresis nonlinearity was approximated by an ESN. Finally, we designed a sliding mode control based on the ESO results with the ESN in the closed loop to precisely control the electric vehicle PMSM systems, and the chattering of the SMC was restrained by $\tanh(\cdot)$. Two different Lyapunov

functions guaranteed the observer validity and the controller effectiveness. The simulations demonstrated that the proposed observer and controller can achieve a good performance and all the signals were uniformly ultimately bounded.

Data Availability

The data used to support the findings of this study are available from the corresponding author upon request.

Conflicts of Interest

The authors declare that they have no conflicts of interest.

Acknowledgments

This work was supported by the Shandong Provincial Natural Science Foundation of China (ZR2017MF048), Shandong Provincial Key Research and Development Project (2019GGX101005 and 2016GGX105013), National Natural Science Foundation of China (61803216), and Shandong University Science and Technology Plan (J17KA214).

References

[1] J. Na, A. S. Chen, G. Herrmann, R. Burke, and C. Brace, "Vehicle engine torque estimation via unknown input observer and adaptive parameter estimation," *IEEE Transactions on Vehicular Technology*, vol. 67, no. 1, pp. 409–422, 2018.

[2] J. Na, Y. Huang, X. Wu, G. Gao, G. Herrmann, and J. Z. Jiang, "Active adaptive estimation and control for vehicle suspensions with prescribed performance," *IEEE Transactions on Control Systems Technology*, vol. 26, no. 6, pp. 2063–2077, 2018.

[3] S. Wang, H. Yu, J. Yu, J. Na, and X. Ren, "Neural-network-based adaptive funnel control for servo mechanisms with unknown dead-zone," *IEEE Transactions on Cybernetics*, pp. 1–12, 2018.

[4] S. Wang, J. Na, X. Ren, H. Yu, and J. Yu, "Unknown input observer-based robust adaptive funnel motion control for nonlinear servomechanisms," *International Journal of Robust and Nonlinear Control*, vol. 28, no. 18, pp. 6163–6179, 2018.

[5] Y. Huang, J. Na, X. Wu, and G. Gao, "Approximation-free control for vehicle active suspensions with hydraulic actuator," *IEEE Transactions on Industrial Electronics*, vol. 65, no. 9, pp. 7258–7267, 2018.

[6] J. Na, Y. Huang, X. Wu, S.-F. Su, and G. Li, "Adaptive finite-time fuzzy control of nonlinear active suspension systems with input delay," *IEEE Transactions on Cybernetics*, pp. 1–12, 2019.

[7] C. Hu, H. Gao, J. Guo et al., "MME-EKF-based path-tracking control of autonomous vehicles considering input saturation," *IEEE Transactions on Vehicular Technology*, vol. 68, no. 6, pp. 5246–5259, 2019.

[8] B. Li, H. Du, W. Li, and B. Zhang, "Integrated trajectory planning and control for obstacle avoidance manoeuvre using non-linear vehicle mp algorithm," *IET Intelligent Transport Systems*, vol. 13, no. 2, pp. 385–397, 2019.

[9] S. Sun, H. Deng, H. Du et al., "A compact variable stiffness and damping shock absorber for vehicle suspension," *IEEE/ASME Transactions on Mechatronics*, vol. 20, no. 5, pp. 2621–2629, 2015.

[10] S. Sun, X. Tang, J. Yang et al., "A new generation of magnetorheological vehicle suspension system with tunable stiffness and damping characteristics," *IEEE Transactions on Industrial Informatics*, vol. 15, no. 8, pp. 4696–4708, 2019.

[11] G. Luo, R. Zhang, Z. Chen, W. Tu, S. Zhang, and R. Kennel, "A novel nonlinear modeling method for permanent-magnet synchronous motors," *IEEE Transactions on Industrial Electronics*, vol. 63, no. 10, pp. 6490–6498, 2016.

[12] D. Egorov, I. Petrov, J. Link, R. Stern, and J. J. Pyrhonen, "Model-based hysteresis loss assessment in PMSMs with ferrite magnets," *IEEE Transactions on Industrial Electronics*, vol. 65, no. 1, pp. 179–188, 2018.

[13] X. Lin, W. Huang, and L. Wang, "SVPWM strategy based on the hysteresis controller of zero-sequence current for three-phase open-end winding PMSM," *IEEE Transactions on Power Electronics*, vol. 34, no. 4, pp. 3474–3486, 2019.

[14] X. Gao, "Adaptive neural control for hysteresis motor driving servo system with Bouc-Wen model," *Complexity*, vol. 2018, Article ID 9765861, 9 pages, 2018.

[15] X. Gao and R. Liu, "Multiscale Chebyshev neural network identification and adaptive control for backlash-like hysteresis system," *Complexity*, vol. 2018, Article ID 1872493, 9 pages, 2018.

[16] Q. Zhu, W. Zhang, J. Na, and B. Sun, "U-model based control design framework for continuous-time systems," in *Proceedings of the 2019 Chinese Control Conference (CCC)*, pp. 106–111, Guangzhou, China, July 2019.

[17] J. Zhang, Q. Zhu, Y. Li, X. Wu, and R. Zhen, "A general U-model based super twisting design procedure for nonlinear polynomial systems," in *Proceedings of the 2017 36th Chinese Control Conference (CCC)*, pp. 3641–3645, Dalian, China, July 2017.

[18] Q. Zhu and L. Guo, "Stable adaptive neurocontrol for nonlinear discrete-time systems," *IEEE Transactions on Neural Networks*, vol. 15, no. 3, pp. 653–662, 2004.

[19] Q. Zhu, D. Zhao, S. Zhang, and P. Narayan, "U-model enhanced dynamic control of a heavy oil pyrolysis/cracking furnace," *IEEE/CAA Journal of Automatica Sinica*, vol. 5, no. 2, pp. 577–586, 2018.

[20] W. Wei, M. Wang, D. Li, M. Zuo, and X. Wang, "Disturbance observer based active and adaptive synchronization of energy resource chaotic system," *ISA Transactions*, vol. 65, pp. 164–173, 2016.

[21] W. He, T. Meng, X. He, and C. Sun, "Iterative learning control for a flapping wing micro aerial vehicle under distributed disturbances," *IEEE Transactions on Cybernetics*, vol. 49, no. 4, pp. 1524–1535, 2019.

[22] Y. Zhu and W. X. Zheng, "Observer-based control for cyber-physical systems with periodic dos attacks via a cyclic switching strategy," *IEEE Transactions on Automatic Control*, p. 1, 2019.

[23] Y. Zhu, W. X. Zheng, and D. Zhou, "Quasi-synchronization of discrete-time Lur'e-type switched systems with parameter mismatches and relaxed PDT constraints," *IEEE Transactions on Automatic Control*, pp. 1–12, 2019.

[24] Y. Zhu and W. X. Zheng, "Multiple lyapunov functions analysis approach for discrete-time switched piecewise-affine systems under dwell-time constraints," *IEEE Transactions on Automatic Control*, p. 1, 2019.

[25] J. Q. Han, "The extended state observer for a class of uncertain systems," *Control and Decision*, vol. 10, no. 1, pp. 85–88, 1995, in Chinese.

[26] W. Xue, W. Bai, S. Yang, K. Song, Y. Huang, and H. Xie, "ADRC with adaptive extended state observer and its application to air-fuel ratio control in gasoline engines," *IEEE Transactions on Industrial Electronics*, vol. 62, no. 9, pp. 5847–5857, 2015.

[27] W. Xue, R. Madonski, K. Lakomy, Z. Gao, and Y. Huang, "Add-on module of active disturbance rejection for set-point tracking of motion control systems," *IEEE Transactions on Industry Applications*, vol. 53, no. 4, pp. 4028–4040, 2017.

[28] Q. Chen, L. Tao, and Y. Nan, "Full-order sliding mode control for high-order nonlinear system based on extended state observer," *Journal of Systems Science and Complexity*, vol. 29, no. 4, pp. 978–990, 2016.

[29] G. Sun, X. Ren, and D. Li, "Neural active disturbance rejection output control of multimotor servomechanism," *IEEE Transactions on Control Systems Technology*, vol. 23, no. 2, pp. 746–753, 2015.

[30] S. Wang, X. Ren, J. Na, and T. Zeng, "Extended-state-observer-based funnel control for nonlinear servomechanisms with prescribed tracking performance," *IEEE Transactions on Automation Science and Engineering*, vol. 14, no. 1, pp. 98–108, 2017.

[31] Q. Chen, L. Shi, J. Na, X. Ren, and Y. Nan, "Adaptive echo state network control for a class of pure-feedback systems with input and output constraints," *Neurocomputing*, vol. 275, pp. 1370–1382, 2018.

[32] G. Sun, D. Li, and X. Ren, "Modified neural dynamic surface approach to output feedback of MIMO nonlinear systems," *IEEE Transactions on Neural Networks and Learning Systems*, vol. 26, no. 2, pp. 224–236, 2015.

[33] S. Wang, J. Na, and X. Ren, "Rise-based asymptotic prescribed performance tracking control of nonlinear servo mechanisms," *IEEE Transactions on Systems, Man, and Cybernetics: Systems*, vol. 48, no. 12, pp. 2359–2370, 2018.

[34] M. Wang, X. Ren, Q. Chen, S. Wang, and X. Gao, "Modified dynamic surface approach with bias torque for multi-motor servomechanism," *Control Engineering Practice*, vol. 50, pp. 57–68, 2016.

[35] S. Wang, X. Ren, J. Na, and X. Gao, "Robust tracking and vibration suppression for nonlinear two-inertia system via modified dynamic surface control with error constraint," *Neurocomputing*, vol. 203, pp. 73–85, 2016.

[36] X. Gao, C. Zhang, C. Zhu, and X. Ren, "Identification and control for hammerstein systems with hysteresis non-linearity," *IET Control Theory & Applications*, vol. 9, no. 13, pp. 1935–1947, 2015.

[37] L. Tao, Q. Chen, Y. Nan, and C. Wu, "Double hyperbolic reaching law with chattering-free and fast convergence," *IEEE Access*, vol. 6, pp. 27717–27725, 2018.

[38] W. Zhao, X. Ren, and S. Wang, "Parameter estimation-based time-varying sliding mode control for multimotor driving servo systems," *IEEE/ASME Transactions on Mechatronics*, vol. 22, no. 5, pp. 2330–2341, 2017.

[39] Q. Chen, S. Xie, M. Sun, and X. He, "Adaptive nonsingular fixed-time attitude stabilization of uncertain spacecraft," *IEEE Transactions on Aerospace and Electronic Systems*, vol. 54, no. 6, pp. 2937–2950, 2018.

[40] S. Bogosyan, M. Gokasan, and D. J. Goering, "A novel model validation and estimation approach for hybrid serial electric vehicles," *IEEE Transactions on Vehicular Technology*, vol. 56, no. 4, pp. 1485–1497, 2007.

[41] J. Na, X. Ren, and D. Zheng, "Adaptive control for nonlinear pure-feedback systems with high-order sliding mode observer," *IEEE Transactions on Neural Networks and Learning Systems*, vol. 24, no. 3, pp. 370–382, 2013.